Theoretical investigation of magnetoelectric effects in $Ba_2CoGe_2O_7$

Kunihiko Yamauchi,[1,2] Paolo Barone,[1] and Silvia Picozzi[1]
[1]*Consiglio Nazionale delle Ricerche (CNR-SPIN), I-67100 L'Aquila, Italy*
[2]*ISIR-SANKEN, Osaka University, 8-1 Mihogaoka, Ibaraki, Osaka 567-0047, Japan*
(Received 27 September 2011; published 31 October 2011)

A joint theoretical approach, combining macroscopic symmetry analysis with microscopic methods (density functional theory and a model cluster Hamiltonian), is employed to shed light on magnetoelectricity in $Ba_2CoGe_2O_7$. The recently reported experimental behavior of polarization guided by a magnetic field [Murakawa *et al.*, Phys. Rev. Lett. **105**, 137202 (2010)] can be predicted on the basis of phenomenological Landau theory. On the microscopic side, two main ingredients are needed for the cross-coupling between magnetic and dipolar degrees of freedom: on-site spin-orbit coupling and the spin-dependent hybridization between O-p and transition metal d states. Structural constraints related to the noncentrosymmetric symmetry and the particular configuration of CoO_4 tetrahedrons provide additional features for a peculiar magnetoelectricity to develop.

DOI: 10.1103/PhysRevB.84.165137 PACS number(s): 75.85.+t, 71.15.Mb, 75.50.Ee, 77.80.−e

I. INTRODUCTION

The magnetoelectric (ME) coupling between magnetic ($\boldsymbol{M}$) and ferroelectric ($\boldsymbol{P}$) order parameters has recently been the object of intense research in the context of ME multiferroic oxides, where magnetism and ferroelectricity appear concomitantly.[1] At odds with conventional ME materials where the induced polarization is linear in the applied magnetic field, as, e.g., prototypical Cr_2O_3,[2] magnetically induced ferroelectrics may display giant and peculiar ME effects.[1] In this respect, several microscopic mechanisms for ME coupling have already been proposed.[3–7] In systems displaying cycloidal or spiral spin structures, the ferroelectric state arises from the spin chirality through a spin-current mechanism.[3] Also referred to as the "inverse Dzyaloshinskii-Moriya interaction" due to the crucial role played by spin-orbit coupling (SOC),[4] this mechanism predicts $\boldsymbol{P} \propto \sum_{ij} \boldsymbol{e}_{ij} \times (\boldsymbol{S}_i \times \boldsymbol{S}_j)$, with $\boldsymbol{S}_i$ and $\boldsymbol{S}_j$ being neighboring spins connected by a vector $\boldsymbol{e}_{ij}$. The largest ME force is expected in the nonrelativistic exchange-striction, or inverse Goodenough-Kanamori, mechanism,[5] which can induce a ferroelectric polarization (even on top of a collinear spin structure) when inversion symmetry is broken, giving $\boldsymbol{P} \propto \sum_{ij} J_{ij}(\boldsymbol{S}_i \cdot \boldsymbol{S}_j)$ with exchange integral J_{ij}. Recently, a third mechanism has been devised, namely spin-dependent p-d hybridization,[6] where the SOC "asymmetrizes" the p-d hybridization between the transition metal (TM) and the surrounding ligands (L); on the basis of a perturbative approach to a three-site (TM-L-TM) cluster model, where the crystal field is assumed *a priori* to have cubic symmetry, Jia *et al.*[7] predicted an electric polarization expressed as $\boldsymbol{P} \propto \sum_{ij} (\boldsymbol{S}_i \cdot \boldsymbol{e}'_j)^2 \boldsymbol{e}'_j$ (where $\boldsymbol{e}'_j$ labels the vectors connecting the TM to the ligands) induced by SOC within the three-fold degenerate t_{2g} manifold.

Since the third mechanism can concomitantly occur with the first or second one (in noncollinear spin structures), it is in general difficult to identify each of these mechanisms. However, it has been recently reported that the TM-L hybridization can be responsible for the polarization observed in $Ba_2CoGe_2O_7$ (BCGO).[8] BCGO shows tetragonal noncentrosymmetric (nonpolar) $P\bar{4}2_1m$ (#113) structure with two inequivalent Co sites, Co1 and Co2 in Fig. 1; below $T_N = 6.7$ K, their spins align in a collinear antiferromagnetic (AFM) structure in the ab plane. Experimentally, a ferroelectric P_c along the c axis has been reported even when $\boldsymbol{H} = 0$.[8,9] When the magnetic field $\boldsymbol{H}$ is applied, $\boldsymbol{P}$ develops finite components along any direction, modulated by the direction and the size of $\boldsymbol{H}$.

In this paper, we present a comprehensive description of ME effects in BCGO, in terms of general symmetry considerations and microscopic methods, that rigorously clarify the role of the proposed mechanism in relation to the lattice and electronic structure of the compound. We show that the magnetic ordering is responsible for the symmetry lowering that allows $\boldsymbol{P}$ to emerge in the otherwise nonpolar (albeit noncentrosymmetric) crystal structure. Microscopically, a local dipole develops on each TM because of the anisotropic p-d hybridization with the surrounding ligands, modulated by the on-site SOC; the onset of $\boldsymbol{P}$ through this mechanism does not necessarily require a specific spin structure, being essentially a single-ion rather than a spin-correlation problem.

II. SYMMETRY ANALYSIS

In order to characterize the peculiar ME effect, we first discuss group theory analysis and its implications in the framework of the Landau theory of phase transitions.[10] The parent $P\bar{4}2_1m1'$ magnetic space group has eight symmetry operations $\{E,\ C_{2(z)},\ 2S_4,\ 2C_{2(x,y)},\ 2\sigma_d\}$ plus time-reversal $(1')$; therefore magnetic ordering leads to a lowered symmetry. By using linear combinations of the two inequivalent Co spins $\boldsymbol{S}_1, \boldsymbol{S}_2$, we define a ferromagnetic (FM) order parameter $\boldsymbol{F} = \boldsymbol{S}_1 + \boldsymbol{S}_2$ and an antiferromagnetic one $\boldsymbol{A} = \boldsymbol{S}_1 - \boldsymbol{S}_2$. The components of the magnetic order parameters $\boldsymbol{M} = \boldsymbol{F}, \boldsymbol{A}$ and of the electric polarization $\boldsymbol{P}$ transform according to the transformation rules given in Table I.

By means of these transformation rules, we can express the thermodynamic free energies in terms of all the possible magnetoelectric coupling terms of the form $\boldsymbol{P} \cdot \boldsymbol{M}^2$ which are invariant under symmetry operations:

$$F_{\mathrm{ME}} = c_{\mathrm{A}} P_c A_a A_b + c_{\mathrm{F}} P_c F_a F_b + c_{\mathrm{AF}} P_c (A_a F_a - A_b F_b) + c_1 (P_a A_a F_c - P_b A_b F_c) + c_2 (P_a A_c F_a - P_b A_c F_b), \quad (1)$$

TABLE I. Matrices of the generators of space group $P\bar{4}2_1m1'$ in the representations spanned by F, A, and P. The group elements denote the identity E, π-rotation C_{2z}, $\pi/2$-rotoinversion S_4^-, screw $C_{2y}+(\frac{1}{2}\frac{1}{2}0)$, and time-reversal $1'$. Labels of irreducible representation (IR) are taken from the ISODISTORT program.[11]

	E	C_{2z}	S_4^-	C_{2y}	$1'$	IR
F_a	$\begin{bmatrix}1&0\\0&1\end{bmatrix}$	$\begin{bmatrix}-1&0\\0&-1\end{bmatrix}$	$\begin{bmatrix}0&1\\-1&0\end{bmatrix}$	$\begin{bmatrix}-1&0\\0&1\end{bmatrix}$	$\begin{bmatrix}-1&0\\0&-1\end{bmatrix}$	$m\Gamma_5E_1^*a$
F_b						$m\Gamma_5E_1^*b$
F_c	1	1	1	-1	-1	$m\Gamma_4A$
A_a	$\begin{bmatrix}1&0\\0&1\end{bmatrix}$	$\begin{bmatrix}-1&0\\0&-1\end{bmatrix}$	$\begin{bmatrix}0&1\\-1&0\end{bmatrix}$	$\begin{bmatrix}1&0\\0&-1\end{bmatrix}$	$\begin{bmatrix}-1&0\\0&-1\end{bmatrix}$	$m\Gamma_5E_2^*b$
A_b						$m\Gamma_5E_2^*a$
A_c	1	1	1	1	-1	$m\Gamma_1A$
P_a	$\begin{bmatrix}1&0\\0&1\end{bmatrix}$	$\begin{bmatrix}-1&0\\0&-1\end{bmatrix}$	$\begin{bmatrix}0&-1\\1&0\end{bmatrix}$	$\begin{bmatrix}-1&0\\0&1\end{bmatrix}$	$\begin{bmatrix}1&0\\0&1\end{bmatrix}$	Γ_5
P_b						Γ_5
P_c	1	1	-1	-1	1	Γ_3

where c_A, c_F, c_1, c_2, and c_{AF} are constants. In order to analyze the ferroelectric response, we also consider the usual dielectric energy, $F_{\rm DE}=-\boldsymbol{P}^2/2\chi$, where χ is the dielectric susceptibility, henceforth set as 1. $\boldsymbol{P}$ is then evaluated at the minima of $F=F_{\rm ME}+F_{\rm DE}$, when $\partial F/\partial P_i=0$ $(i=a,b,c)$, reading

$$\begin{aligned} P_a &= c_1A_aF_c + c_2A_cF_a,\\ P_b &= -c_1A_bF_c - c_2A_cF_b,\\ P_c &= c_{\rm A}A_aA_b + c_{\rm F}F_aF_b + c_{\rm AF}(A_aF_a - A_bF_b). \end{aligned} \tag{2}$$

Note that only the first term of P_c originates purely from the AFM order, explaining the observed spontaneous $\boldsymbol{P}$, whereas other components are allowed only in the presence of the FM order parameter. In this respect, Eq. (1) implies a coupling between the FM and AFM orders,[12] with a consequent weak ferromagnetism (WFM) showing a net magnetization in the ab plane, as postulated in Refs. 13 and 9. However, our density functional theory results show only a tiny spin canting ($\theta \ll 0.1^\circ$) after optimizing the spin structure starting from the AFM configuration, which does not support quantitatively the existence of WFM.

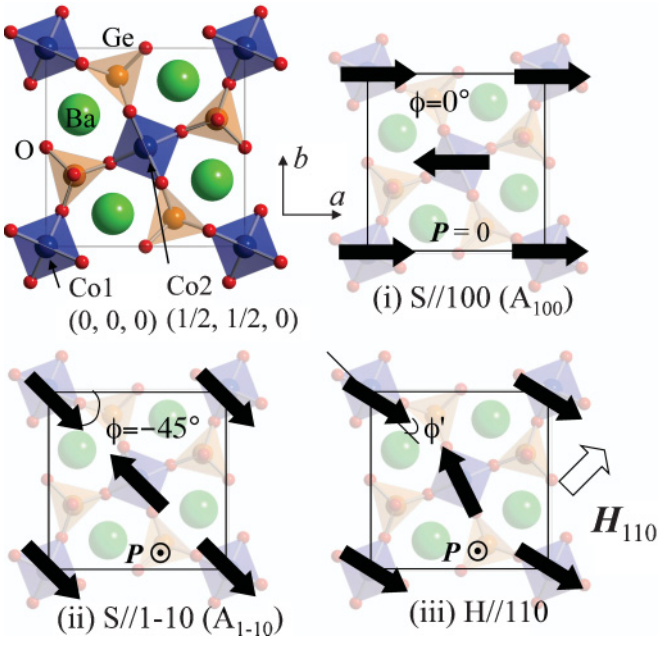

FIG. 1. (Color online) Crystal structure in the ab plane; Co and Ge ions (both located in O_4 tetrahedron) lie in $c=0$ planes, whereas the Ba ion lies in $c=1/2$ planes. Co spin configurations: (i) [100]-directed and (ii) [110]-directed (collinear) AFM and (iii) noncollinear spin-canted under applied $\boldsymbol{H}$//110.

We focus on the P_c behavior, assuming a canted AFM configuration under an applied magnetic field; i.e., we first simultaneously rotate counterclockwise two antiparallel Co spins in the ab plane with an angle ϕ from the a axis, then we cant spins by an angle ϕ', as depicted in Fig. 1. Accordingly, we set $\boldsymbol{S}_1=S[\cos(\phi+\phi'),\ \sin(\phi+\phi'),0]$ and $\boldsymbol{S}_2=S[-\cos(\phi-\phi'),\ -\sin(\phi-\phi'),0]$, ending up with

$$\begin{aligned} P_c(\phi) &= 2S^2\sin 2\phi(c_{\rm A}\cos^2\phi' - c_{\rm F}\sin^2\phi' - c_{\rm AF}\sin 2\phi')\\ &= 2\alpha S^2\sin 2\phi\cos(2\phi'-\beta), \end{aligned} \tag{3}$$

where $\alpha^2=c_{\rm AF}^2+(c_{\rm A}+c_{\rm F})^2/2$ and $\tan\beta=-(c_{\rm A}+c_{\rm F})/2c_{\rm AF}$. By neglecting the canting angle ϕ', Eq. (3) perfectly reproduces the experimentally observed dependence of polarization on the spin angle. A polarization $P_c\propto\sin 2\phi$ has been reported at $T=2$ K and $H=1$ T in Ref. 8. A spontaneous P_c can therefore be induced in the A_{110} ($A_{1\text{–}10}$) order but not in the A_{100} (A_{010}) one (cf. Fig. 1). We rationalize this behavior by noticing that the symmetries which prohibit P_c (e.g., C_{2y} rotation) in the nonmagnetic group, which is nonpolar although it lacks inversion symmetry, are broken by the A_{110} magnetic order. Applying $\boldsymbol{H}$ on top of the A_{110} order results in a further symmetry reduction. Indeed, A_{110} order shows $2_z'$ point group, which allows nonzero α_{13}, α_{23}, α_{31}, and α_{32} linear ME components[14] in such a way that P_a and P_b can be induced by applying H_z. Finally, Eq. (3) at fixed ϕ gives the simple ϕ' dependence $P_c(\phi')\propto\alpha\cos(2\phi'-\beta)$, where the phase shift depends on the nonzero $c_{\rm AF}$ coefficient.

III. DENSITY FUNCTIONAL THEORY ANALYSIS

In order to quantitatively confirm the ME behavior and to investigate its microscopic mechanism, we performed density functional theory (DFT) calculations using VASP[15] with the GGA-PBE potential (and also checking our results by using the GGA + U[16] potential with $U=3$ or 5 eV for the Co-d state). Due to the lack of experimental information on structural parameters, we considered the $Ca_2CoSi_2O_7$ structure[17] and

TABLE II. Magnetic anisotropy energy (meV/Co) obtained by comparing the total energy with different spin directions under SOC and for different values of U in the GGA $+U$ scheme. Spin and orbital moment (μ_B) are also reported for S//(100). In the rightmost column we report the calculated P_c (μC/m^2) for $S(L)$//110 with fixed atomic structure.

	$E(100)$	$E(110)$	$E(001)$	S	L	P_c
bare GGA	0	0.00	+0.17	2.53	0.17	12.7
$U = 3$ eV	0	0.00	+0.16	2.61	0.17	12.2
$U = 5$ eV	0	−0.31	+0.65	2.75	0.24	10.6

optimize it by substituting atoms (Ca $\leftrightarrow$ Ba, Si $\leftrightarrow$ Ge) without SOC. The optimized structure shows $a = b = 8.28$ Å and $c = 5.58$ Å and a tilting angle of the CoO_4 tetrahedron given by $\kappa = 23.9°$, consistent with experimental values of $a = b = 8.41$ Å and $c = 5.54$ Å (Ref. 9) and $\kappa = 24°$.[8]

In CoO_4 tetrahedra, the Co^{2+} ion shows orbital-quenched $e_g^{2\uparrow} t_{2g}^{3\uparrow} e_g^{2\downarrow} t_{2g}^{0\downarrow}$ states, which cause a very small magnetic anisotropy, as shown in Table II. The observed magnetically easy ab plane and hard c axis are consistent with experiments (S//010 from neutron diffraction[18]). The small magnetic anisotropy energy (MAE) in the ab plane explains why the spins easily follow an applied $\boldsymbol{H}$: even under a small magnetic field, the spins flop to be perpendicular to $\boldsymbol{H}$ and then cant in order to reduce the Zeeman energy. We then evaluated the ME effect as the change of $\boldsymbol{P}$ (calculated via Berry phases[19]) induced by suitable rotations of Co spins with respect to the crystalline axes in the fixed nonpolar crystal structure, thus mimicking the effect of an applied $\boldsymbol{H}$.

Imposing the collinear AFM configuration, we first simultaneously rotate the Co spins in the ab plane by an angle ϕ. In Fig. 2(a) we show P_c as a function of ϕ, consistent with both experiments and the previously discussed Landau analysis in which $P_c \propto \sin 2\phi$. The calculated polarization, which displays a maximum value $P_c = 12.7\ \mu$C/m^2 at A_{1-10}, originates here from a purely electronic contribution via SOC and is further enhanced when atomic internal coordinates are optimized in the A_{1-10} configuration, as discussed later. We look then at the spin-canting effect induced by an applied field H_{110}. In Fig. 2(b) we show the change in P_c induced by artificially canting the spins by an angle ϕ', starting from the A_{1-10} AFM configuration. In agreement with the Landau theory analysis, P_c evolves as $\cos 2(\phi' - 22.7°) + \text{constant}$, displaying a peak at $\phi' \sim \kappa$. The $\boldsymbol{P}$-$\boldsymbol{H}$ curve shown in the inset in Fig. 2(b)—first increasing with $\boldsymbol{H}$ and then decreasing and changing its sign—denotes an atypical nonlinear ME trend,

TABLE III. P_c at different canting angle ϕ', calculated in the fixed nonpolar structure (first line) and with optimized (opt.) internal atomic coordinates (second line). The largest experimental value of P_c is $\sim$120 μC/m^2.[8]

	ϕ'		
P_c (μC/m^2)	0°	30°	90°
fixed structure	12.7	17.6	−12.7
opt. structure	39.8	57.7	−38.9

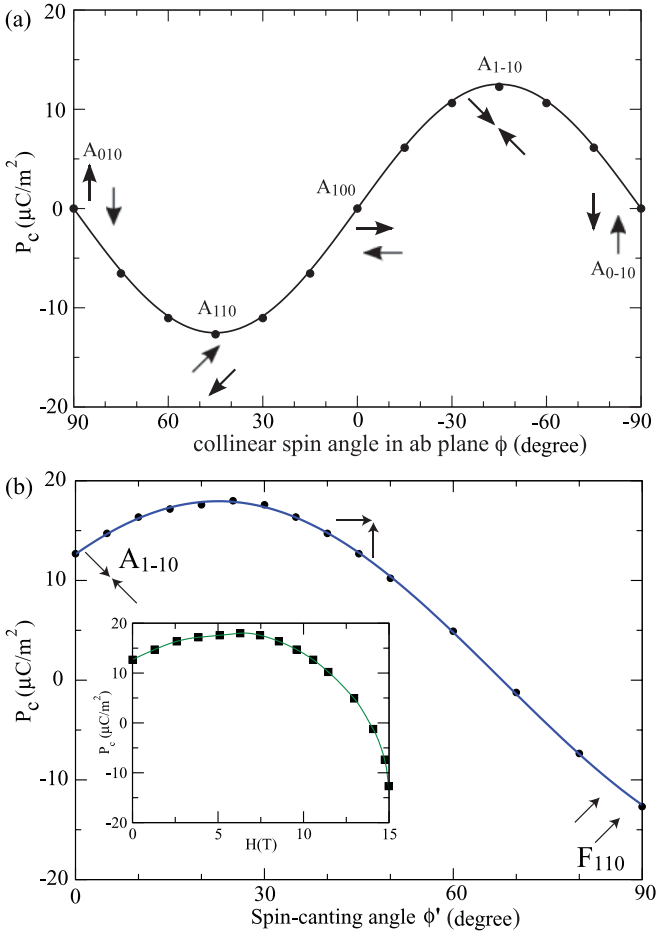

FIG. 2. (Color online) (a) DFT results for $\boldsymbol{P}_c$ as a function of the *collinear* spin angle ϕ in the ab plane, fitted to $f(\phi) = -a \sin 2\phi$, with $a = 12.7$ (solid line). Spin configurations in the ab plane shown by arrows. (b) DFT results for $\boldsymbol{P}_c$ as a function of the *noncollinear* spin-canting angle ϕ' in the ab plane, fitted to $f(\phi') = a \cos 2(\phi' - b) + c$, with $a = 17.9$, $b = 22.7$, and $c = 0.06$ (solid line). Inset: $\boldsymbol{P}_c$ as a function of magnetic field $\boldsymbol{H}$, assuming the experimentally measured magnetic susceptibility $\chi = F/H_{110} \approx 0.25\ \mu_B$/T per Co.[8]

which emerges from the symmetry properties of BCGO rather than from high-order terms in the free energy expansion in series of the electric and magnetic fields.

Although the trend of P shows good agreement with experiments,[8] its size is one order of magnitude smaller. This deviation is reduced when the atomic structure is optimized in the canted-AFM configuration, as shown in Table III. Such a dominant ionic contribution to the SOC-induced polarization is also seen in ferroelectric $TbMnO_3$.[20] This means that ferroelectricity is strongly coupled, through magnetism, with lattice distortions in a sort of magnetically induced piezoelectric effect.

IV. SINGLE-SITE SOC-INDUCED ME EFFECT

The role of local SOC and of anisotropic p-d hybridization in BCGO as well as its single-ion character can be further clarified by considering a cluster Hamiltonian for a single CoO_4 tetrahedron. By neglecting contributions from the energetically deeper majority-spin states, but taking fully in

account the crystal field of the tetrahedral oxygen cage, the Hamiltonian for the CoO_4 cluster consists of four terms, $H = H_d + H_p + H_{pd} + H_{SOC}$, where

$$\begin{aligned} H_d &= \Delta \sum_{\alpha} d_{\alpha}^{\dagger} d_{\alpha}, \\ H_p &= \varepsilon_p \sum_{l,\beta} p_{l,\beta}^{\dagger} p_{l,\beta}, \\ H_{pd} &= \sum_{\alpha,\beta,l} V_{\alpha\beta l} \left(d_{\alpha}^{\dagger} \, p_{l,\beta} + \text{h.c.} \right), \\ H_{SOC} &= \lambda \sum_{\alpha,\alpha'} \langle \alpha | \, L \cdot S \, | \alpha' \rangle \, d_{\alpha}^{\dagger} d_{\alpha'}. \end{aligned} \tag{4}$$

Hereafter we assume $\varepsilon_p = 0$ as the energy reference and $\Delta = \varepsilon_d - \varepsilon_p$ as the charge-transfer energy. Subscripts α and β refer to the $d = xy$, yz, zx, x^2-y^2, $3z^2$-r^2 and $p = x,y,z$ orbitals involved, whereas $l = 1, \ldots, 4$ labels the four oxygens surrounding the Co ion, located at $\boldsymbol{R}_l = (1,1,-1),(-1,-1,-1),(1,-1,1)$, and $(-1,1,1)$ in the local reference system with Co in the origin. The hybridization matrix $V_{\alpha\beta l}$ depends on the d and p orbitals involved (with σ or π bonding) and on the relative positions of the ions; we adopted the Slater-Koster parametrization,[21] assuming $t_{pd\sigma} = 1.3$ eV, $\Delta = 5.5$ eV,[22] and $t_{pd\pi} = -0.45\, t_{pd\sigma}$.[23] With this parametrization, the tetrahedral crystal-field splitting between lower-energy two-fold degenerate e_g and higher-energy three-fold degenerate t_{2g} states is recovered. The matrix elements $\mathcal{H}^{soc}(\alpha,\alpha') = \langle \alpha | \, L \cdot S \, | \alpha' \rangle$ entering the last term read

$$\mathcal{H}^{soc} = \frac{1}{2} \begin{pmatrix} 0 & i\cos\theta & -i\sin\theta\sin\phi & -i\sin\theta\cos\phi & -i\sqrt{3}\sin\theta\cos\phi \\ -i\cos\theta & 0 & i\sin\theta\cos\phi & -i\sin\theta\sin\phi & i\sqrt{3}\sin\theta\sin\phi \\ i\sin\theta\sin\phi & -i\sin\theta\cos\phi & 0 & i\cos\theta & 0 \\ i\sin\theta\cos\phi & i\sin\theta\sin\phi & -i\cos\theta & 0 & 0 \\ i\sqrt{3}\sin\theta\cos\phi & -i\sqrt{3}\sin\theta\sin\phi & 0 & 0 & 0 \end{pmatrix}, \tag{5}$$

as a function of the polar and azimuthal angles (θ,ϕ) defining a local reference for the spin-quantization axis.[24] We assume $\lambda = 0.021$ eV, the free Co ion spin-orbit coupling value. The Hamiltonian is then exactly solved by means of standard diagonalization techniques for different values of the azimuthal angle ϕ at $\theta = 90^\circ$, mimicking spins rotating in the ab plane.

SOC-induced mixing of the local d levels lifts the degeneracies in the e_g and t_{2g} manifolds, respectively, and implies different hybridizations with the ligand oxygens, which may ultimately induce a local dipole moment by varying their local occupancies $\rho_{O(l)} = \sum_{\beta} \langle \, p_{l,\beta}^{\dagger} \, p_{l,\beta} \, \rangle$. As shown in Fig. 3, rotating the spin in the ab plane by the azimuthal angle ϕ differentiates between lower- and upper-lying oxygens, with $\rho_{up,lo} \propto \pm \sin(2\phi)$. Then a local dipole $\boldsymbol{p} = (e/4) \sum_l \rho_{O(l)} \boldsymbol{R}_l$ may develop in the tetrahedron only along c, proportional to the charge difference $\Delta\rho_O = \rho_{up} - \rho_{lo}$, i.e., $p_c \propto 2 \sin 2\phi$, in excellent agreement with the predicted functional form $\boldsymbol{P} \propto \sum_{ij} (\boldsymbol{S}_i \cdot \boldsymbol{e}'_j)^2 \, \boldsymbol{e}'_j$.[6–8] Furthermore, we can estimate the d-orbital mixing on the Co site by looking at the orbital occupancies $\rho_{\alpha}^{Co} = \langle \, d_{\alpha}^{\dagger} \, d_{\alpha} \, \rangle$, shown in Fig. 3. Even if the two occupied states have prevalent $d_{x^2-y^2}, d_{3z^2-r^2}$ characters, a small mixing occurs via SOC with (mostly) d_{yz}, d_{zx} orbitals, being $\rho_{yz} \propto \cos^2\phi$, $\rho_{zx} \propto \sin^2\phi$; i.e., the most occupied is the one perpendicular to the spin-quantization axis. These findings are in excellent agreement with DFT calculations, as shown in Fig. 4 and in Table IV, where the hierarchy of d-orbital occupancies at selected values of the spin direction is confirmed. Such a mixing of local d-levels nicely

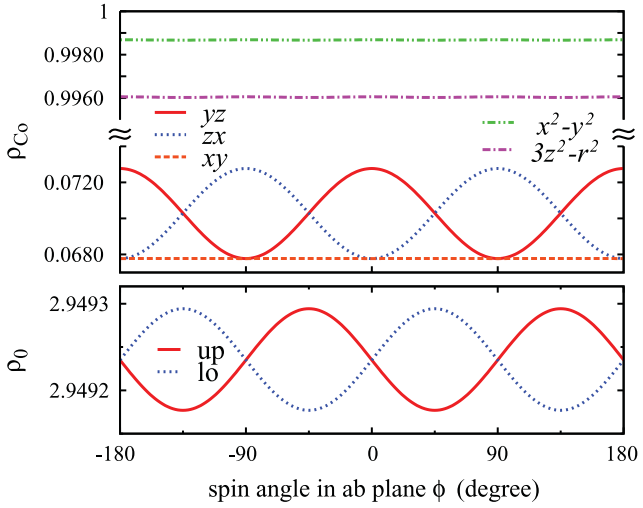

FIG. 3. (Color online) Model results. (Bottom) Electron density of upper- and lower-lying oxygens, ρ_O, in the tetrahedron model as a function of the azimuthal angle ϕ at $\theta = 90^\circ$. (Top) Orbital occupancy on Co, ρ_{α}^{Co}, as a function of ϕ.

TABLE IV. DFT-calculated $3d$ orbital-decomposed occupancy (in percentage, with spin states summed up) with different SOC enhancement factors λ (0 = without SOC, ×1 = with standard SOC, and ×10 = with the SOC term artificially enhanced by a factor of 10) for different $\boldsymbol{S}$ directions in the local xyz frame. Significant changes of the occupancy are highlighted in boldface type.

λ	$\boldsymbol{M}$	xy	yz	zx	$3z^2$-r^2	x^2-y^2
0	—	50.0	50.0	50.0	100.0	100.0
×1	$\boldsymbol{S}//\boldsymbol{x}$	50.0	**50.2**	50.0	99.9	99.9
×1	$\boldsymbol{S}//\boldsymbol{y}$	50.0	50.0	**50.2**	99.9	99.9
×10	$\boldsymbol{S}//\boldsymbol{x}$	49.5	**61.7**	49.7	92.8	96.3
×10	$\boldsymbol{S}//\boldsymbol{y}$	49.5	49.7	**61.7**	92.8	96.3

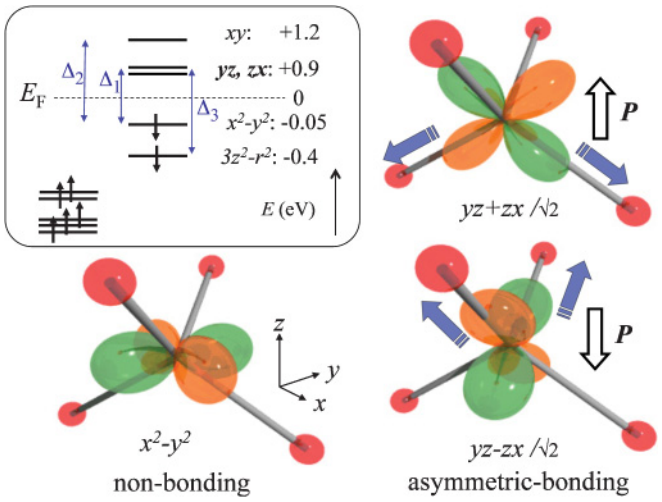

FIG. 4. (Color online) Bonding nature of the d orbital in O_4 tetrahedron and induced local polarization. Via SOC, asymmetrically bonded orbital states are mixed with nonbonding occupied states. Inset: DFT-calculated energy levels of orbital states. Possible SOC mixing in minority spin states are shown with energy difference Δ_i.

explains why the p_c size is maximum at $\phi = \pm 45^\circ$, when the Co spin is parallel either to the upper- or to the lower-lying oxygen bond; indeed, as pictorially shown in Fig. 4, the composition of yz and zx orbitals, whose partial occupation is activated by the e_g-t_{2g} spin-orbit coupling, has an asymmetric bonding nature in the tetrahedron, i.e., nonbonding with upper ligands and bonding with lower ligands or vice versa.

The evolution of P_c with the spin angle in BCGO can be nicely deduced from our model by considering two CoO_4 tetrahedra tilted by κ. In the AFM collinear configuration we find $P_c \propto p_{c1}(\phi + \kappa) + p_{c2}(\phi + \pi - \kappa) = 2\cos\kappa \sin 2\phi$. Analogously, in order to mimic the effect of the external H_{110}, we can define the canting angles as $\phi_1' = \phi + \kappa - \pi/4$ and $\phi_2' = -\phi + \kappa + 3\pi/4$, yielding $P_c(\phi') \propto \cos 2(\phi' - \kappa)$, in excellent agreement with experiments and DFT results.

V. CONCLUSIONS

We shed light on the mechanism underlying peculiar magnetoelectric effects in $Ba_2CoGe_2O_7$, by combining different theoretical approaches and explicitly taking into account the microscopic atomic arrangement and symmetries of the compound. Our Landau phenomenological theory shows the following: (i) On top of noncentrosymmetric nonpolar $P\bar{4}2_1m$ symmetry in the nonmagnetic crystal structure, a collinear antiferromagnetic spin configuration with in-plane spins allows an electric polarization along the z axis. (ii) Upon applying an external magnetic field, the induced noncollinear spin-canting well reproduces the experimentally observed peculiar trend of polarization related to the tilting angle between CoO_4 tetrahedrons. In order to have quantitative estimates, we perform relativistic *ab initio* calculations and highlight the delicate interplay between orbital occupation and local magnetic anisotropy, resulting in an excellent match with available experiments. Furthermore, as a proof that the microscopic origin of magnetoelectricity is based on two relevant ingredients (i.e., the anisotropic p-d hybridization between Co and O states and the on-site spin-orbit coupling), we built a simple cluster model that, by taking into account the crystal-field effects relevant for BCGO, is sufficient to nicely explain magnetoelectric effects and shows that the functional form $\boldsymbol{P} \propto \sum_{ij}(\boldsymbol{S}_i \cdot \boldsymbol{e}_j')^2\, \boldsymbol{e}_j'$, predicted for t_{2g} systems with cubic symmetry,[7] also applies to systems with tetrahedral symmetry through SOC-induced e_g-t_{2g}-orbital mixing. In conclusion, our analysis put forward $Ba_2CoGe_2O_7$ as a prototype of the class of materials where the interplay between magnetism and ferroelectricity is based on spin-dependent p-d hybridization, as recently suggested in the literature.[8]

Recently we have become aware of a similar symmetry analysis[25] performed for BCGO by Toledano *et al*. However, their focus is on toroidal moments, whereas ours is on the combination of single-ion anisotropy and p-d hybridization (derived from density functional and tight-binding models) as the microscopic mechanism driving magnetoelectricity.

ACKNOWLEDGMENTS

We thank J. Manuel Perez-Mato for fruitful discussions. The research leading to these results has received funding from the EU Seventh Framework Programme (FP7/2007-2013) under ERC Grant No. 203523-BISMUTH and from JST, CREST "Creation of Innovative Functions of Intelligent Materials on the Basis of the Element Strategy." Computational support from the Caspur Supercomputing Center (Rome) is gratefully acknowledged.

[1] M. Fiebig, J. Phys. D **38**, R123 (2005).
[2] J. Íñiguez, Phys. Rev. Lett. **101**, 117201 (2008).
[3] H. Katsura, N. Nagaosa, and A. V. Balatsky, Phys. Rev. Lett. **95**, 057205 (2005).
[4] I. A. Sergienko and E. Dagotto, Phys. Rev. B **73**, 094434 (2006).
[5] S. Picozzi *et al*., Phys. Rev. Lett. **99**, 227201 (2007).
[6] T. Arima, J. Phys. Soc. Jpn. **76**, 073702 (2007).
[7] C. Jia, S. Onoda, N. Nagaosa, and J. H. Han, Phys. Rev. B **76**, 144424 (2007).
[8] H. Murakawa, Y. Onose, S. Miyahara, N. Furukawa, and Y. Tokura, Phys. Rev. Lett. **105**, 137202 (2010).
[9] H. T. Yi *et al*., Appl. Phys. Lett. **92**, 212904 (2008).
[10] L. D. Landau and E. M. Lifshitz, *Statistical Physics, Part I* (Pergamon, Oxford, 1980).
[11] B. J. Campbell *et al*., J. Appl. Cryst. **39**, 607 (2006).
[12] J. M. Perez-Mato and J. L. Ribeiro, Acta Cryst. A **67**, 264 (2011).
[13] T. Sato, T. Masuda, and K. Uchinokura, Physica B **329**, 880 (2003).
[14] *International Tables for Crystallography, Vol. D, Physical Properties of Crystals*, edited by A. Authier (Kluwer Academic, Dordrecht, 2003).
[15] G. Kresse and J. Furthmüller, Phys. Rev. B **54**, 11169 (1996).

[16]V. I. Anisimov, F. Aryasetiawan, and A. I. Lichtenstein, J. Phys. Condens. Matter **9**, 767 (1997).
[17]K. Hagiya and M. Ohmasa, Acta Cryst. B **49**, 172 (1993).
[18]A. Zheludev, T. Sato, T. Masuda, K. Uchinokura, G. Shirane, and B. Roessli, Phys. Rev. B **68**, 024428 (2003).
[19]R. D. King-Smith and D. Vanderbilt, Phys. Rev. B **47**, 1651 (1993); R. Resta, Rev. Mod. Phys. **66**, 899 (1994).
[20]A. Malashevich and D. Vanderbilt, Phys. Rev. Lett. **101**, 037210 (2008).
[21]J. C. Slater and G. F. Koster, Phys. Rev. **94**, 1498 (1954).
[22]J. van Elp and A. Tanaka, Phys. Rev. B **60**, 5331 (1999).
[23]W. A. Harrison, *Electronic Structure and the Properties of Solids* (Freeman, San Francisco, 1980).
[24]H. Takayama, K. Bohnen, and P. Fulde, Phys. Rev. B **14**, 2287 (1976).
[25]P. Toledano, D. D. Khalyavin and L. C. Chapon, Phys. Rev. B **84**, 094421 (2011).